

A metabolically engineered bacterium controls autoimmunity and inflammation by remodeling the pro-inflammatory microenvironment

Jugal Kishore Das^{a#}, Fengguang Guo^{a#}, Carrie Hunt^b, Shelby Steinmeyer^c, Julia A Plocica^a, Koichi S. Kobayashi^{a,d}, Yufang Ding^c, Arul Jayaraman^c, Thomas A Ficht^e, Robert C. Alaniz^a, Paul de Figueiredo^{a,e}, and Jianxun Song^{ib a}

^aDepartment of Microbial Pathogenesis and Immunology, Texas A&M University Health Science Center, Bryan, TX, USA; ^bDepartment of Entomology, Texas A&M University, College Station, Bryan, TX, USA; ^cDepartment of Chemical Engineering, Texas A&M University, College Station, Bryan, TX, USA; ^dDepartment of Immunology, Graduate School of Medicine, Hokkaido University, Sapporo, Japan; ^eDepartment of Veterinary Pathobiology, Texas A&M University, College Station, Bryan, TX, USA

ABSTRACT

Immunotherapy has led to impressive advances in the treatment of autoimmune and pro-inflammatory disorders; yet, its clinical outcomes remain limited by a variety of factors including the pro-inflammatory microenvironment (IME). Discovering effective immunomodulatory agents, and the mechanisms by which they control disease, will lead to innovative strategies for enhancing the effectiveness of current immunotherapeutic approaches. We have metabolically engineered an attenuated bacterial strain (i.e., *Brucella melitensis* 16M $\Delta vj b R$, Bm $\Delta vj b R::tnaA$) to produce indole, a tryptophan metabolite that controls the fate and function of regulatory T (T_{reg}) cells. We demonstrated that treatment with Bm $\Delta vj b R::tnaA$ polarized macrophages (M ϕ) which produced anti-inflammatory cytokines (e.g., IL-10) and promoted T_{reg} function; moreover, when combined with adoptive cell transfer (ACT) of T_{reg} cells, a single treatment with our engineered bacterial strain dramatically reduced the incidence and score of autoimmune arthritis and decreased joint damage. These findings show how a metabolically engineered bacterium can constitute a powerful vehicle for improving the efficacy of immunotherapy, defeating autoimmunity, and reducing inflammation by remodeling the IME and augmenting T_{reg} cell function.

ARTICLE HISTORY

Received 13 April 2022
Revised 12 October 2022
Accepted 26 October 2022

KEYWORDS

Microbe;
immunometabolism;
regulatory T cells;
autoimmunity; inflammation

Introduction


Recent advances in cancer immunotherapy have not only revolutionized the field of tumor immunology,^{1–3} but also rejuvenated research into exploring novel strategies for autoimmune immunotherapy. Numerous studies have demonstrated promising results using immunotherapy to treat autoimmune and pro-inflammatory disorders.^{4–6} Nevertheless, despite advances in the field of autoimmune-immunotherapy, including regulatory T cell (T_{reg})-based therapy, the efficacy and benefits of these approaches remain less satisfactory due to limited *in vivo* T_{reg} expansion and persistence, the pro-inflammatory microenvironment (IME), and insufficient T_{reg} trafficking to inflamed sites. In addition, immune dysregulation of the IME contributes to disease.⁷ Immunotherapeutic combinations may produce

greater efficacy, and thus strategies that circumvent these barriers are urgently needed.

To address this need, we developed and tested an intervention that combined two innovations. First, although a therapeutic role for live attenuated bacterial vaccines in addressing infectious diseases is undeniable and appreciated in cancer immunotherapy, the use of bacterial agents to manage autoimmune and pro-inflammatory diseases remains limited.^{8–10} Second, a growing number of microbiota-specific products and metabolites have novel immunologic properties that constitute one mechanism whereby the microbiota influence host health and disease.^{11–14} We therefore developed a metabolically engineered bacterial vaccine strain to produce immunomodulatory metabolites that improve autoimmunity and inflammation.

CONTACT Paul de Figueiredo  pjdefigueiredo@tamu.edu  Department of Microbial Pathogenesis and Immunology, Texas A&M University Health Science Center, Bryan, TX, USA; Robert C. Alaniz  robert_alaniz@tamu.edu; Thomas A Ficht  tficht@tamu.edu  Department of Veterinary Pathobiology, Texas A&M University, College Station, Bryan, TX, USA; Jianxun Song  jus35@tamu.edu

[#]These authors contributed equally to this work.

 Supplemental data for this article can be accessed online at <https://doi.org/10.1080/19490976.2022.2143222>

© 2022 The Author(s). Published with license by Taylor & Francis Group, LLC.

This is an Open Access article distributed under the terms of the Creative Commons Attribution License (<http://creativecommons.org/licenses/by/4.0/>), which permits unrestricted use, distribution, and reproduction in any medium, provided the original work is properly cited.

Results

For the bacterial vector, we selected an attenuated strain of *Brucella melitensis* that harbors a deletion in *vjbR*, a master regulator of virulence (*BmΔvjbR*).¹⁵ Like other Gram-negative organisms, *Brucella* strains express a lipopolysaccharide (LPS) lacking endotoxin activity. Importantly, *BmΔvjbR* has been shown to be safe in immunocompetent and immunocompromised mice,¹⁶ goats,¹⁷ sheep,¹⁸ and non-human primates.¹⁹ We have also shown that *BmΔvjbR* can combat cancer in a murine model by remodeling the tumor microenvironment (TME) to a pro-inflammatory state.¹⁵ Moreover, when *BmΔvjbR* treatment was combined with adoptive cell transfer (ACT) of tumor antigen (Ag)-specific CD8⁺ T cells, tumor growth and proliferation were dramatically impaired.¹⁵ Conversely, in the current studies, we engineered *BmΔvjbR* to express tryptophanase (*tnaA*); i.e., *BmΔvjbR::tnaA*, to produce the tryptophan metabolite indole, a molecule that modulates the fate and function of T_{regs}.²⁰

We have reported that indole, when used at a range of physiologic concentrations, suppresses several inflammatory characteristics in immune and nonimmune cells,²¹ and also augments T_{reg} differentiation.²² Consistent with our previous reports, we demonstrated that indole suppressed TNF- α production in CD11b⁺ spleen cells after *E. coli* LPS (eLPS) and heat-inactivated *Salmonella* Typhimurium [HKST] stimulation (Figure 1a & Figure 1b) and dampened their activation by suppressing Akt and ERK signaling pathways in response to microbial agonists (eLPS and HKST) (Fig. S1a). In addition, indole augmented the differentiation of naive CD4⁺CD25⁻ T cells into induced T_{regs} (iT_{regs}) measured by FoxP3 *in vitro* in a dose dependent manner (Figure 1c & Figure 1d). These findings were consistent with our earlier reports,¹⁵ and were comparable to results from studies using the microbiota metabolite butyrate, albeit with distinct dose-dependency.²³ Based on these findings, we hypothesized that indole would ameliorate immune-mediated inflammation in autoimmune and pro-inflammatory diseases.

Thus, we examined whether indole reduces autoimmune responses in a murine collagen-induced arthritis (CIA) model. We delivered 20 mg/kg

indole in corn-oil to C57BL/6 mice (N = 5) having CIA and assessed the arthritis score in these mice compared to untreated control (PBS; N = 5). First, we showed that the severity of CIA was significantly attenuated in indole treated mice, which exhibited clinical scores of 0.8 ± 0.2 (means \pm SEM) at (Day 50), compared to 1.6 ± 0.5 in controls (Figure 1e). However, a single dose of indole only showed a slight decrease in inflammation. Similarly, single dose treatment did not induce significant alterations in the infiltration of T_{reg} cells as assessed by confocal microscopy (Figure 1f & Figure 1g). These findings were in striking contrast to our *ex vivo* experimental findings, which indicated that indole significantly promoted the expansion of CD4⁺FoxP3⁺ T_{reg} cells and enhanced their activation by increased expression of PD-1 an immunosuppressive molecule, compared to the controls ($p < .001$), in cells derived from the mouse lymph nodes (LNs) and spleen (Figure 1h & Figure 1i). Based on our *in vivo* and *ex vivo* findings, we hypothesized that the sustained delivery of indole in a bacterial vector may greatly improve the durability of the molecule's immunomodulatory effects, resulting in an attenuation of autoimmunity and inflammation in CIA. To test this hypothesis, we engineered a safe live-attenuated bacterial strain (i.e., *BmΔvjbR::tnaA*) to constitutively produce indole (Figure 2a-c). First, we observed that the engineered bacterial strain survived mainly in the spleen for 7 days and liver and kidney for 3 dpi (Figure 2d). The bacteria did not penetrate the joints of the mice (Figure 2d). Second, we observed low-level immunogenicity by detection of anti-*Brucella* IgG antibodies from 3 to 21 dpi of the bacteria (Figure 2e). Moreover, we also determined that the colonies of *BmΔvjbR::tnaA* bacterial strain recovered from mice challenged with collagen-induced arthritis (CIA) at 7 dpi could still produce indole (Figure 2f). Further, cytokine array profiling analyses showed that *BmΔvjbR::tnaA* induced the expression of IL-10 in macrophages (M ϕ) (Figure 3a & Fig. S2a), which promotes the activities of T_{reg} cells and reduces autoimmunity and inflammation. Strikingly, *BmΔvjbR::tnaA* also significantly ($p < .01$) reduced the expression of additional pro-inflammatory cytokines like IL-6, IL-1 β and TNF- α in macrophages (M ϕ) compared to *BmΔvjbR* parental strain (Figure 3a). We also found that

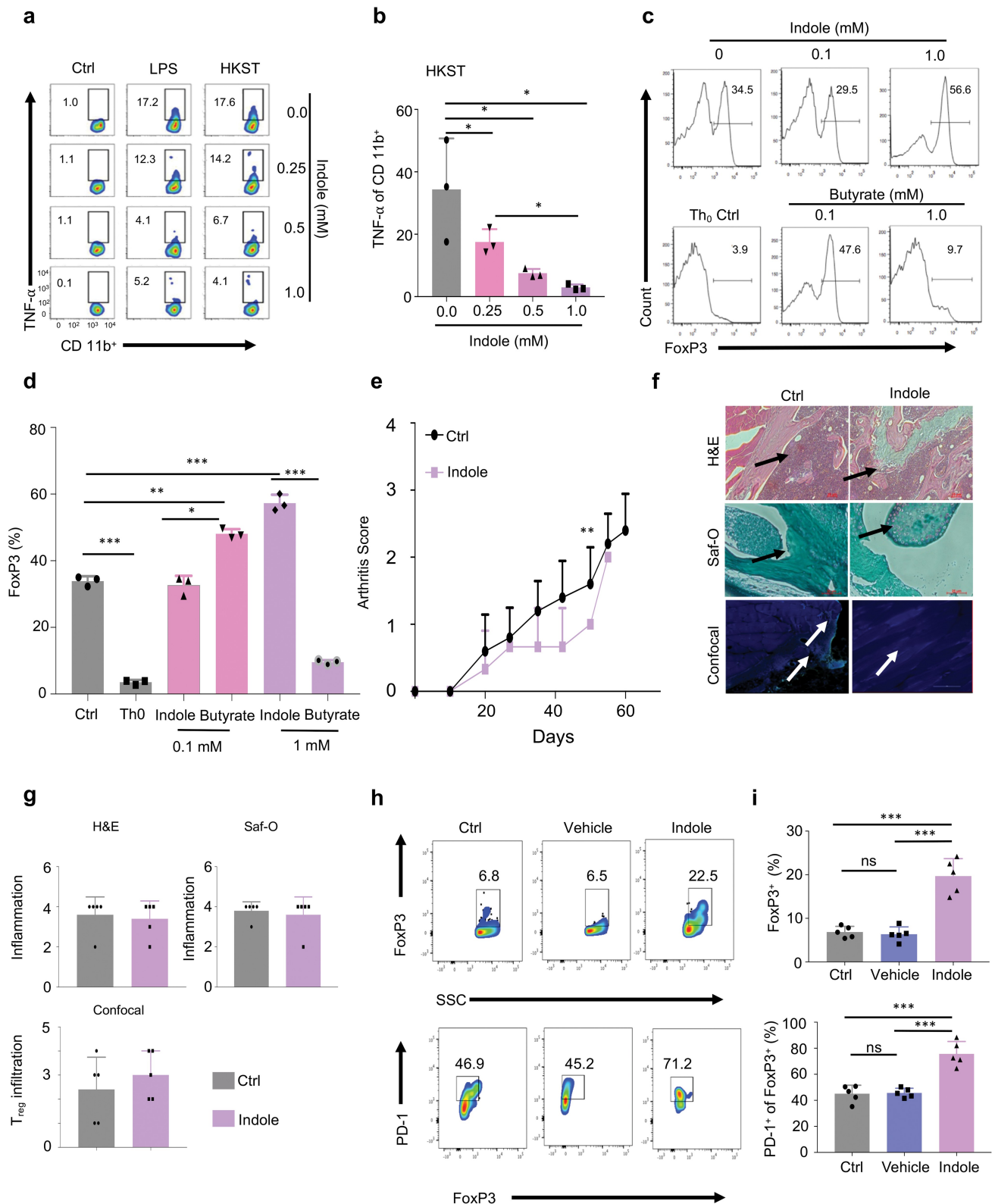


Figure 1. Indole treatment dampens inflammation and promotes Treg cell expansion and activity. a, Representative flow cytometric dot-plot analysis of the effect of indole on CD11b⁺ cells. 0.25, 0.5, or 1.0 mM indole was dissolved in DMF for the representative experimental flow cytometric analysis. b, Graphical representation of flow cytometric dot-plots derived from 3 independent experiments of heat killed *Salmonella Typhimurium* (HKST) group. c, flow cytometric histograms representing the dose-dependent indole induced differentiation of Treg cells. Experiment (N=3) was performed under Treg cell skew conditions ([TGF- β] = 2 ng/mL, [IL-2] = 100 U/mL). Th₀ control represents non-Treg cell skew conditions. Butyrate was used as a control metabolite. d, Graphical representation of the effect of indole on the differentiation of Treg cells. e, Graphical representation of the effects of indole alone on CIA in mice (N=5). f, Representative images of H&E, Safranin O (Saf-O) stained tissues, and confocal microscopy of knee tissues of CIA mice on day 60 post induction of arthritis. Arrows indicate areas of infiltration of immune cells (H&E), cartilage-integrity (Saf-O) and Treg cell infiltration (confocal microscopy).

BmΔvjbR::tnaA, when co-cultured with bone marrow-derived Mφ (BMDMs), not only significantly reduced the total CD4⁺ T cells ($p < .001$) but also reduced the production of the pro-inflammatory cytokines such as TNF-α and IFN-γ ($p < .001$) compared to the *BmΔvjbR* parental strain (Figure 3b). Moreover, *BmΔvjbR::tnaA* promoted the expansion of T_{reg} cells and significantly enhanced their activity as assessed by IL-10 production ($p < .001$) and PD-1 expression ($p < .01$) (Fig. S2a). Third, in the CIA model (Fig S1b), a significant reduction in arthritis score and incidence was observed following treatment with *BmΔvjbR::tnaA*. This amelioration of autoimmunity and inflammation was further augmented when *BmΔvjbR::tnaA* treatment was combined with ACT of T_{reg} cells (Figure 3c). Fourth, we observed significantly ($p < .01$) reduced numbers of infiltrating inflammatory cells into the joints of mice treated with *BmΔvjbR::tnaA*. This effect was further enhanced by *BmΔvjbR::tnaA* treatment followed by the ACT of T_{reg} cells compared to the controls ($p < .001$) (Figure 3d). Finally, mice treated with *BmΔvjbR::tnaA* showed reduced infiltrates in the joint and intact cartilages as evidenced by H&E analysis and Safranin O (Saf-O) staining of knee cross-sections (60 days post collagen administration). Notably, these findings were further attenuated by addition of ACT of T_{reg} cells (Figure 3d). There was also a significant reduction in the total CD4⁺ T cell proportion in the joints and a significant increase in T_{reg} cell proportion in mice treated with *BmΔvjbR::tnaA* compared to controls ($p < .001$; Figure 3e). Since it is unlikely that *BmΔvjbR::tnaA* bacteria will be used prior to the onset of arthritis in the clinic, we conducted an experiment to assess the impact of our strategy in treatment of established CIA by starting the administration of bacteria and T_{reg} cells, 3 weeks post collagen administration. Our results indicate that *BmΔvjbR::tnaA* combined with ACT of T_{reg} cells

significantly dampens the progression of the disease but is not sufficient to completely cure the disease (Fig S3a and S3b).

To identify the mechanism by which *BmΔvjbR::tnaA* might be acting, we conducted a multiparametric CyTEK analysis from the cells isolated from the spleen, LNs and/or the knee and ankle joints of control, ACT with T_{reg} cells only, or ACT with T_{reg} cells plus *BmΔvjbR::tnaA* groups. We found that the *BmΔvjbR::tnaA* reduced the proportion of B cells (Figure 3f, Figure 3g, Fig. S2b, and Table S1) in addition to promoting T_{reg} cell expansion. Overall, our results indicate that *BmΔvjbR::tnaA* remodels the IME and facilitates the expansion and suppressive function of T_{reg} cells as depicted in the illustration (Figure 4). Our results also indicate that *BmΔvjbR::tnaA* may modulate B cell-mediated immunity in our murine model of CIA to alleviate symptoms of arthritis in these mice.

Discussion

Several strategies have been employed to enhance the efficacy of live attenuated bacterial vaccines.^{13,14} However, bacterial vaccines producing immunomodulatory metabolites that alter the immunological tolerance and the IME have not been previously reported. Our work features both conceptual and methodological innovations. First, this work provides the first description of a live attenuated vaccine whose metabolism has been reprogrammed to amplify anti-autoimmune/inflammation activity.

Second, this study provides the first description of how combining a single dose of an engineered live attenuated bacterial vaccine strain with the ACT of T_{reg} cells can achieve potent therapeutic outcomes. Previous studies have demonstrated the efficacy of the administration of a single dose of polyclonal T_{reg} cells in controlling CIA in DBA/1 mouse model.²⁴ Moreover, Sun et al have also

Intracellular FoxP3 staining (green) was used to denote Treg cells. g, Quantitative analysis of H&E, Saf-O and Treg cell infiltration from confocal microscopy sections of Control (Ctrl) and indole-treated mice. h, Flow cytometric dot-plot analysis of PD-1 and FoxP3 in ex vivo activated CD4⁺ T cells isolated from LNs and spleen of C57BL/6 mice. Exposure to indole drives these cells towards higher Treg cell phenotype by increased FoxP3 expression. Vehicle (control) indicates corn-oil which was used as a solvent for indole. i, Graphical representation of FoxP3 derived from the flow cytometric dot-plots of CD4⁺ T cells exposed to indole. Graphical representation of PD-1+ FoxP3+ T cells (%) from the flow cytometric dot-plots. Data represent means ± SD. Student's t-test or Tukey's multiple comparisons test was applied for statistical analysis. *, **, ***: significance at $p < 0.05, 0.01, 0.001$.

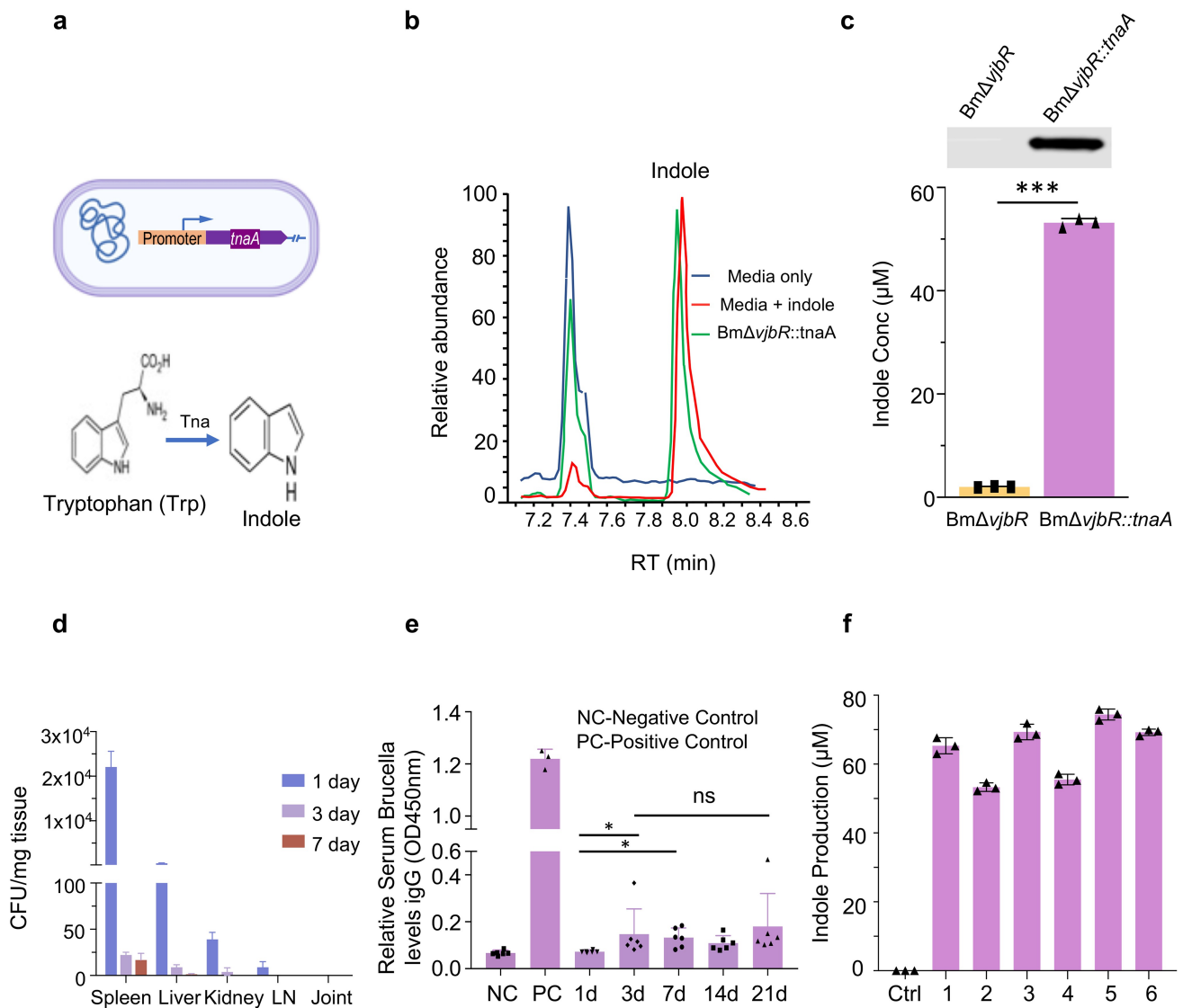


Figure 2. *BmΔvjbR* is engineered to produce indole. a, Schematic representation of the engineered *BmΔvjbR::tnaA* harboring a plasmid carrying a *tnaA* expression cassette. The indole biosynthesis pathway is depicted in the figure. TnaA catalyzes the conversion of tryptophan to indole. b, Mass spectrometric analysis of indole production by engineered *BmΔvjbR::tnaA*. c, Western blotting analysis of the expression of *tnaA* protein in the parental strain compared with the engineered *BmΔvjbR::tnaA* strain. Graphical representation of the comparative analysis of indole production by *BmΔvjbR* parental bacterial strain and the engineered *BmΔvjbR::tnaA* strain. d, Colonization of engineered *BmΔvjbR::tnaA* in the spleen, liver, kidney and lymph-nodes of CIA mice. The bacteria colonized in all the organs for 3 days post-inoculation and could be observed only in the spleen for 7 days. The numbers represent single colonies grown on the plate. The bacteria recovered at 7 days post infection from mice still could produce indole. e, Serum ELISA analysis of anti-Brucella IgG production. The positive and negative controls were used as per the manufacturer's instructions. f, Indole production of *BmΔvjbR::tnaA* bacteria recovered from CIA mice. Data represents means \pm SD. Student's t-test or Tukey's multiple comparisons test was applied for statistical analysis. *, ***: significance at $p < 0.05$, 0.001.

demonstrated the efficacy of antigen specific T_{reg} cells in suppressing inflammation of CIA in C57BL/6 mouse model.²⁵ However, these studies are limited by the durability of anti-inflammatory responses of antigen specific T_{reg} cells and the possibility of reversion to pathogenic effector T-cell type. Moreover, the studies did not show the

efficacy of therapeutic adoptive T_{reg} cell therapy in controlling CIA in mice. Although previous studies have reported the efficacy of ACT of T_{reg} cells in autoimmune diseases²⁶ our study is the first report showing the enhanced efficacy of combinatorial adoptive immunotherapy in C57BL/6 CIA mouse model. We have also shown that ACT of T_{reg} cells

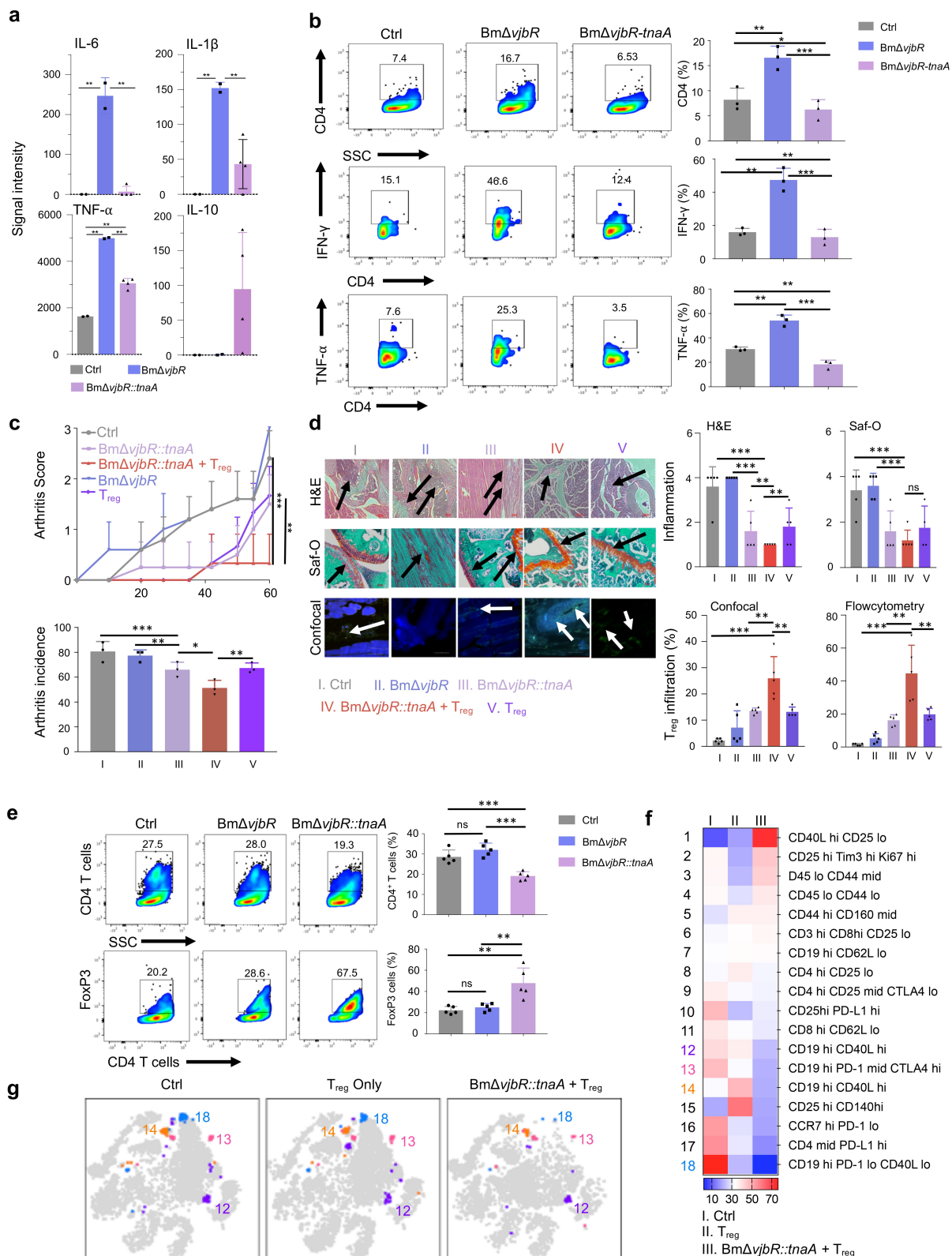


Figure 3. Bm Δ vjbR::tnaA significantly dampens inflammation and reduces arthritis in murine CIA model which is augmented by adoptive cell transfer (ACT) of Treg cells. a, Cytokine arrays were used to measure pro-inflammatory cytokines produced by control, Bm Δ vjbR, and Bm Δ vjbR::tnaA treated BMDMs. b, Flow cytometric analysis of IFN- γ and TNF- α of T cells co-cultured with BMDMs. BMDMs were treated with either Bm Δ vjbR::tnaA or Bm Δ vjbR and then co-cultured with CD4⁺ T cells derived from pooled LNs and spleen of C57BL/6 mice for the assay. c, Arthritis score and arthritis incidence in CIA C57BL/6 mice from control (Ctrl, gray bar); Bm Δ vjbR (blue bar); Bm Δ vjbR::tnaA (pink bar); Bm Δ vjbR::tnaA followed by ACT of Treg cells (Treg, red bar) and ACT of Treg cells only; (N=5 in each group). d, Representative images of H&E, Saf-O staining, and confocal microscopy from mouse knees on day 60 post CIA induction. Arrows indicate areas of infiltration of immune cells (H&E), cartilage-integrity (Saf-O) and Treg cell infiltration (confocal microscopy). Intracellular FoxP3 staining (green) was used to denote Treg cells. Quantitative analysis of Treg cell infiltration and inflammation scores from these mice are

not only prevents CIA in mice, but also controls the progression of the disease when administered subsequent to the onset of the disease. More importantly, our study also provides an overview of the immune landscape in the CIA mouse model and shows how the adoption of our combinatorial strategy breaks immunological tolerance and ameliorates CIA.

Third, we demonstrate how the genetic tractability of Bm Δ vjbR can be exploited to engineer vaccines with novel properties. Although in this work, we focused on metabolic reprogramming of the bacterium, we envision that future iterations of the Bm Δ vjbR::tnaA vaccine will include engineered auto antigens (Ags) to boost persistent auto Ag-specific T_{reg} cell responses. Fourth, this work showed that a single administration of indole did not succeed as a stand-alone agent. However, this limitation was circumvented by indole delivery using our engineered bacterial vector. Bm Δ vjbR::tnaA may offer improved pharmacodynamics for indole by sustained production levels and effects *in vivo* versus indole alone. Moreover, we showed that the separate individual beneficial effects of Bm Δ vjbR and indole act synergistically *in vivo*.

Finally, the natural localization of Bm Δ vjbR to leukocytes enabled Bm Δ vjbR::tnaA to provide improved targeted indole delivery and a higher local effective indole concentration in contrast to the untargeted and transient nature of indole as a single agent. In sum, our work presents an attractive new avenue for the development of anti-autoimmunity/inflammation vaccines.

Methods

CIA induction

CIA was induced as described previously with minor modifications.²⁷ Briefly, male C57BL/6

mice were injected with an emulsion of 100 μ l of chick type II collagen (Chondrex; 100 μ g) in Complete Freund's Adjuvant (CFA; Chondrex) using a glass tuberculin syringe with 26-gauge needle. The mice were then assessed for development of joint inflammation and clinical arthritis score until Day 60 as described previously.²⁸

Indole treatment in CIA mouse

CIA was induced in male C57BL/6 mice. On Day 7 after the CIA induction, mice were intraperitoneally (*i.p.*) injected with 20 mg/kg indole or corn oil (vehicle control).

Bacterial culture

Bm Δ vjbR or Bm Δ vjbR::tnaA were cultivated and prepared for experimentation as previously described.¹⁵

Engineering indole-producing Bm Δ vjbR::tnaA strain

To generate an indole producing attenuated Bm Δ vjbR strain, we cloned an *Escherichia coli* (*E. coli*) tnaA gene into a broad range bacteria expression plasmid (pBBR1MCS6Y)²⁹ and transferred the plasmid to Bm Δ vjbR.

Indole Detection and quantification

The indole production by Bm Δ vjbR::tnaA was detected by liquid chromatography–mass spectrometry (LC-MS). After 24 hr cultivation of the bacteria in Tryptic Soy Broth (TSB) medium at 37°C, the metabolites were extracted using ice-cold methanol for LC-MS assay. Liquid chromatography tandem mass spectrometry analysis was performed on a TSQ Altis triple quadrupole mass spectrometer

also shown. e, Cells from knee and ankle joints were collected from CIA-induced mouse groups (Ctrl, Bm Δ vjbR, and Bm Δ vjbR::tnaA combined with ACT of Treg cells). These cells were then stained and quantified by flow cytometry using markers for CD4+ T cells (upper panel) and intracellular staining of FoxP3 (Treg cells) (lower panel). f, CIA-induced mice were treated with PBS (Ctrl), ACT of Treg cells only (Treg cells only; N=5), or Bm Δ vjbR::tnaA combined with ACT of Treg cells (N=5). Cells from the spleen, LNs and joints were stained with 21 markers and measured by CyTEK aurora flow cytometry. Heatmap shows immune cell profiles in different treatment groups of mice (scale bar represents percentage of cell in each treatment group within each cell type). g, viSNE map shows the four subtypes of B cells differentially expressed in the treated group of mice. Data represent means \pm SD. Student's t-test or Tukey's multiple comparisons test was applied for statistical analysis. *, **, ***: significance at $p < 0.05, 0.01, 0.001$.

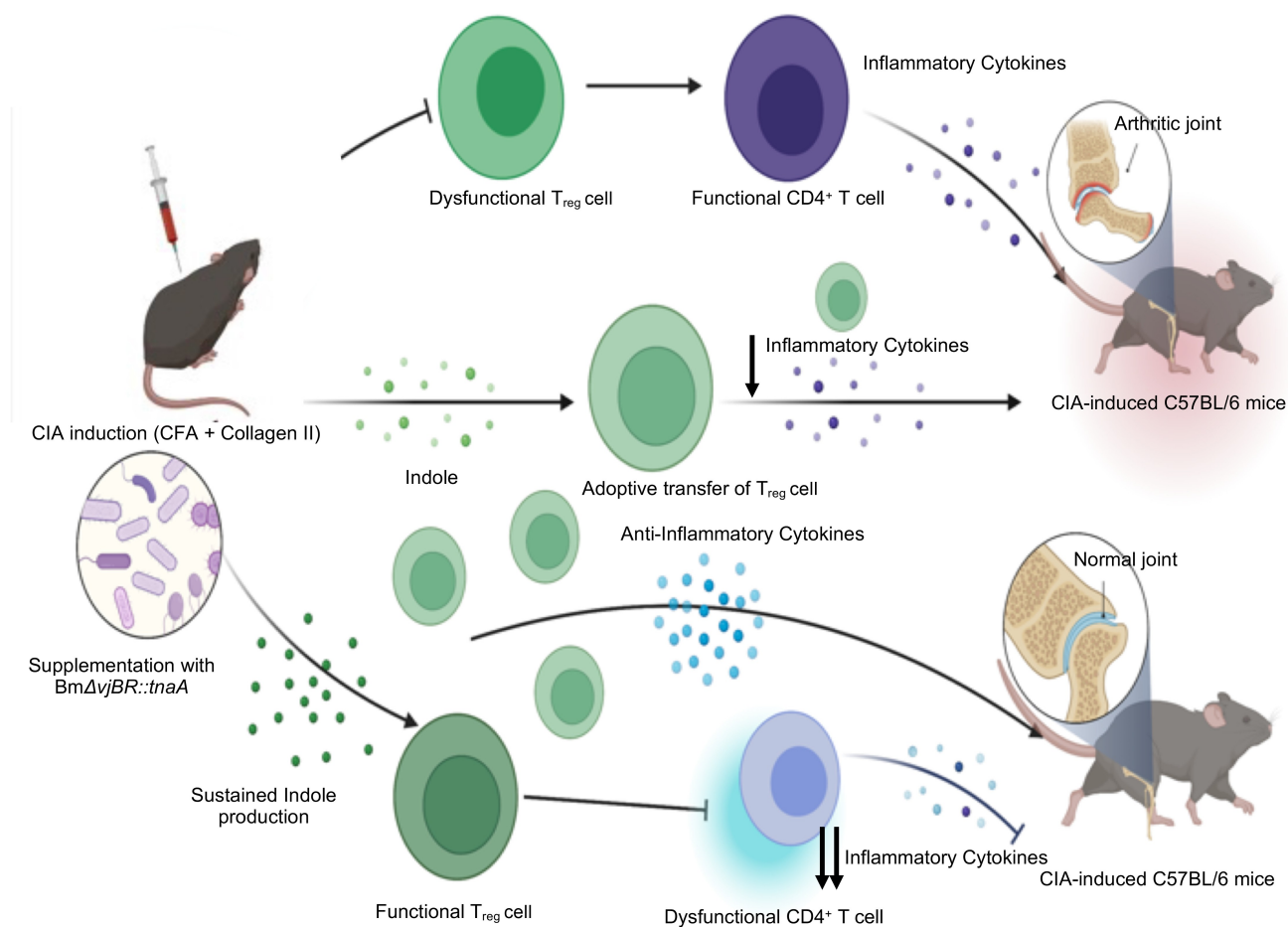


Figure 4. Schematic representation of amelioration of CIA in C57BL/6 mice by engineered bacteria. The illustration depicts the process of amelioration of CIA in C57BL/6 mice by the engineered *BmΔvjbR::tnaA* bacterial strain. C57BL/6 mice may harbor a microbiome deficient in production of the metabolite indole. When challenged with the CIA, these mice rapidly develop arthritis due to dysfunctional Tregs and rapid expansion of CD4⁺ effector T cells. However, when *BmΔvjbR::tnaA* bacteria are administered to mice bearing CIA, the Treg activity is substantially increased and the pathogenic activity of CD4⁺ effector T cells is compromised, which results in amelioration of joint inflammation and improved symptoms. This activity is greatly augmented by an ACT of T_{regs}.

(Thermo Scientific, Waltham, MA) coupled to a binary pump HPLC (Vanquish, Thermo Scientific). The indole concentration was measured using an indole assay kit following the manufacturer's protocol (Sigma-Aldrich).

***BmΔvjbR::tnaA* treatment and ACT of T_{reg} cells**

CIA was induced in male C57BL/6 mice. On Day 7 after the CIA induction, mice were intravenously (*i.v.*) injected with 5.0×10^7 live *BmΔvjbR::tnaA* or PBS control. In the *BmΔvjbR::tnaA* + T_{reg} cell combinatorial treatment group, mice (N = 5) were adoptively transferred with 2.5×10^6 CD4⁺CD25⁺ T_{reg} cells derived from donor lymph nodes (LNs)

and spleen of naive C57BL/6 mice, one week after the *BmΔvjbR::tnaA* administration.

For treatment of established CIA, mice were injected with 5.0×10^7 live *BmΔvjbR::tnaA* or indole/PBS control on Day 21 post injection of CFA + Collagen followed by T_{reg} cell injection on Day 25.

Enumeration of *BmΔvjbR::tnaA* recovered from CIA mice

BmΔvjbR::tnaA (5.0×10^7) were *i.v.* injected into C57BL/6 mice and the bacterial distribution and survival were analyzed by colony forming unit (CFU) assay. The mice were sacrificed at 1, 3, 7, 14, and 21 dpi of bacteria. The spleen, liver, LNs

and joints were homogenized and plated on Tryptic Soy Agar (TSA) plates supplemented with chloramphenicol. The CFU was enumerated after 3-day post-cultivation of the bacteria.

Serum ELISA for detection of BmΔ specific IgG antibody

The CIA induced C57BL/6 mice were sacrificed at 1, 3, 7, 14, and 21 dpi of BmΔ*vjbR* and/or BmΔ*vjbR::tnaA* bacteria. Blood samples were collected from the mice and serum was isolated by coagulation of the blood at room temperature followed by centrifugation at $2,000 \times g$ for 20 minutes. The serum sample was assayed for anti-BmΔ*vjbR* IgG antibody by using mouse *Brucella* antibody IgG ELISA kit following manufacturer's instructions (AFG Scientific).

Cytokine responses

BMDMs were seeded in 24-well plates at a concentration of 2.0×10^5 cells/well in DMEM without antibiotics. After overnight culture, the cells were inoculated with BmΔ*vjbR* or BmΔ*vjbR::tnaA* bacteria at a multiplicity of infection of 20. At 24 h post-treatment, cellular supernatant was collected and analyzed for the presence of cytokines/chemokines by using a Proteome Profiler Mouse Cytokine Array Kit (R&D Systems, Inc.).

Flow cytometric analysis

Cell staining and flow cytometric analysis were performed as described previously¹⁵ using the described labeling reagents. Briefly, surface and intracellular staining was performed on the single-cell suspensions and analyzed using LSR Fortessa cell analyzer (BD). The spleen, joints and LNs were also processed and stained similarly with antibodies listed in Table S2, and data was acquired on CyTEK aurora flow cytometer (Cytex Biosciences). For multiparametric analysis, the data were analyzed with FlowJo v10 and represented as heatmaps and tSNE plots.

Histology and immunofluorescence

Mice were humanely sacrificed on day 60 after induction of CIA, and tissue sections were analyzed as previously described.²⁷ Briefly, the hind foot paws and knees were removed and fixed in 10% formalin and decalcified in Formical-4 (Decal chemical, Tallman, NY). The fixed tissue sections were then stained with H&E and/or Safranin O fast green (Saf-O) stain. The H&E and Saf-O stained sections were then assessed by a semiquantitative system of 0 to 4 as described previously. Immunofluorescent staining and microscopy were performed on the deparaffinized sections by using FITC anti-mouse FoxP3 antibody (Ab) for T_{reg} cells and DAPI as nuclear stain.

Statistical analysis

One-Way ANOVA, Student's *t*-test, or Tukey's multiple comparisons test was performed for statistical analysis between the groups. All analyses were performed in GraphPad Prism v9. A *p* value of <0.05 was considered statistically significant.

Key messages

What is already known about this subject?

- BmΔ*vjbR* has been shown to be safe in immunocompetent and immunocompromised animals.
- Microbiota-specific products and metabolites have novel immunologic properties.

What does this study add?

- Novel bacterial platform produce immunomodulatory metabolites that alter the immunological tolerance and the IME.

How might this impact on clinical practice or future developments?

- Combining a single dose of an engineered live attenuated bacterial therapeutic with ACT of T_{regs} can achieve potent therapeutic outcomes.

The use of engineered bacterial agents is an innovative and malleable approach to manage autoimmune and pro-inflammatory diseases.

Acknowledgment

We thank Robbie Moore from COM-CAF, Malea Murphy from IMIL, Sankar P. Chaki from TAMH-CVM, and Elizabeth Bustamante from TAMU-HSC, and the Immunomonitoring Core facility at Houston Methodist Hospital-Texas Medical Center for their technical supports.

Disclosure statement

The authors have declared that no conflict of interest exists.

Funding

This work was supported by funding from NIH R01AI121180, R21AI167793, and R01CA221867 (R01AI121180, R21AI167793 and R01CA221867 to J.S., R01AI110642 to R. A., R01HD084339 to T.A.F., and R01AI141607-01A1 to P.D. F.), NSF DBI1532188 and NSF0854684 DBI1532188, and NSF0854684 to P.D.F.

ORCID

Jianxun Song  <http://orcid.org/0000-0002-9734-6176>

Ethical approval information

All the animal experiments were performed in compliance with the regulations of The Texas A&M University Animal Care Committee (IACUC #2017-0332) and in accordance with the guidelines of the Association for the Assessment and Accreditation of Laboratory Animal Care.

Contributorship

JS, PDF, RCA, TF, JKD and FG conceived and designed the experiments. JKD and FG performed the experiments and analyzed the data. JS, PDF, JKD, FG, RCA, TF, CH, SH, JAP, KSK and AJ wrote the manuscript and provided critical feedback. JS and PDF supervised the research. All the authors read and approved the final manuscript.

Data sharing statement

All data relevant to the study are included in the article.

References

- Zhang Y, Zhang Z. The history and advances in cancer immunotherapy: understanding the characteristics of tumor-infiltrating immune cells and their therapeutic implications. *Cell Mol Immunol.* 2020;17(8):807–821. doi:10.1038/s41423-020-0488-6.
- J-q F, Wang M-F, Chen H-L, Shang D, Das JK, Song J. Current advances and outlooks in immunotherapy for pancreatic ductal adenocarcinoma. *Mol Cancer.* 2020;19(1):32. doi:10.1186/s12943-020-01151-3.
- Fan J, Das JK, Xiong X, Chen H, Song J. Development of CAR-T Cell persistence in adoptive immunotherapy of solid tumors. *Front Oncol.* 2021;10. doi:10.3389/fonc.2020.574860.
- Kansal R, Richardson N, Neeli I, Khawaja S, Chamberlain D, Ghani M, et al. Sustained B cell depletion by CD19-targeted CAR T cells is a highly effective treatment for murine lupus. *Sci Transl Med.* 2019;11(482). PubMed PMID: 30842314; PubMed Central PMCID: PMC68201923. doi:10.1126/scitranslmed.aav1648.
- Dall’Era M, Pauli ML, Remedios K, Taravati K, Sandoval PM, Putnam AL, et al. Adoptive Treg cell therapy in a patient with systemic lupus erythematosus *Arthritis Rheumatol* 2019;71:431–440Epub 2018/10/03. doi: 10.1002/art.40737. PubMed PMID: 30277008; PubMed Central PMCID: PMC6447289
- Haque M, Lei F, Xiong X, Das JK, Ren X, Fang D, et al. Epub 2019/02/20. doi: 10.1172/jci.insight.126471. PubMed PMID: 30777937; PubMed Central PMCID: PMC6483657. Stem cell-derived tissue-associated regulatory T cells suppress the activity of pathogenic cells in autoimmune diabetes. *JCI Insight.* 2019;4(7).
- Sumida T, Lincoln MR, Ukeje CM, Rodriguez DM, Akazawa H, Noda T, et al. Activated beta-catenin in Foxp3(+) regulatory T cells links inflammatory environments to autoimmunity *Nat Immunol* 2018;19:1391–1402Epub 20181029. doi: 10.1038/s41590-018-0236-6. PubMed PMID: 30374130; PubMed Central PMCID: PMC6240373
- Walter J, Armet AM, Finlay BB, Shanahan F. Establishing or exaggerating causality for the gut microbiome: lessons from human microbiota-associated rodents. *Cell.* 2020;180(2):221–232. Epub 2020/01/25. doi: 10.1016/j.cell.2019.12.025. PubMed PMID: 31978342.
- Gill T, Brooks SR, Rosenbaum JT, Asquith M, Colbert RA. Novel inter-omic analysis reveals relationships between diverse gut microbiota and host immune dysregulation in HLA-B27-Induced experimental spondyloarthritis. *Arthritis Rheumatol.* 2019;71(11):1849–1857. Epub 2019/06/20. doi: 10.1002/art.41018. PubMed PMID: 31216122; PubMed Central PMCID: PMC67603391.
- Bender E. Could a bacteria-stuffed pill cure autoimmune diseases? *Nature.* 2020;577(7792):S12–S3. Epub 2020/01/31. doi: 10.1038/d41586-020-00197-z. PubMed PMID: 31996821.
- Han S, Van Treuren W, Fischer CR, Merrill BD, DeFelice BC, Sanchez JM, et al. A metabolomics pipeline for the mechanistic interrogation of the gut microbiome *Nature* 2021;595:415–420Epub 20210714. doi:

- 10.1038/s41586-021-03707-9. PubMed PMID: 3426 2212
12. Henrick BM, Rodriguez L, Lakshmikanth T, Pou C, Henckel E, Arzoomand A, et al. Bifidobacteria-mediated immune system imprinting early in life *Cell* **2021**;184:3884–98 e11Epub 20210617. doi: [10.1016/j.cell.2021.05.030](https://doi.org/10.1016/j.cell.2021.05.030). PubMed PMID: 34143954
 13. Zegarra-Ruiz DF, El Beidaq A, Iniguez AJ, Lubrano Di Ricco M, Manfredo Vieira S, Ruff WE, et al. A diet-sensitive commensal lactobacillus strain mediates TLR7-dependent systemic autoimmunity *Cell Host Microbe* **2019**;25:113–27 e6Epub 2018/12/26. doi: [10.1016/j.chom.2018.11.009](https://doi.org/10.1016/j.chom.2018.11.009). PubMed PMID: 30581114; PubMed Central PMCID: PMC6377154
 14. Montgomery TL, Kunstner A, Kennedy JJ, Fang Q, Asarian L, Culp-Hill R, et al. Interactions between host genetics and gut microbiota determine susceptibility to CNS autoimmunity *Proc Natl Acad Sci U S A* **2020**;117:27516–27527Epub 2020/10/21. doi: [10.1073/pnas.2002817117](https://doi.org/10.1073/pnas.2002817117). PubMed PMID: 33077601; PubMed Central PMCID: PMC67959502
 15. Guo F, Das JK, Kobayashi KS, Qin QM, AF T, Alaniz RC, et al. Live attenuated bacterium limits cancer resistance to CAR-T therapy by remodeling the tumor microenvironment. *J Immunother Cancer*. **2022**;10(1). PubMed PMID: 34987022; PubMed Central PMCID: PMC68734016. doi:[10.1136/jitc-2021-003760](https://doi.org/10.1136/jitc-2021-003760).
 16. Costa LF, Cabello AL, Batista DFA, Chaki SP, de Figueiredo P, da Paixao TA, et al. The candidate vaccine strain *Brucella ovis* abcBA is protective against *Brucella melitensis* infection in mice *Microbiol Immunol* **2020**;64:730–736Epub 20201008. doi: [10.1111/1348-0421.12850](https://doi.org/10.1111/1348-0421.12850). PubMed PMID: 32965738
 17. Castano-Zubieta MR, Rossetti CA, Garcia-Gonzalez DG, Maurizio E, Hensel ME, Rice-Ficht AC, et al. Evaluation of the safety profile of the vaccine candidate *Brucella melitensis* 16MΔ*vjbR* strain in goats *Vaccine* **2021**;39:617–625Epub 20201213. doi: [10.1016/j.vaccine.2020.11.033](https://doi.org/10.1016/j.vaccine.2020.11.033). Epub 20201213
 18. Hensel ME, Garcia-Gonzalez DG, Chaki SP, Hartwig A, Gordy PW, Bowen R, et al. Epub 20200513. doi: [10.1128/mSphere.00120-20](https://doi.org/10.1128/mSphere.00120-20). Epub 20200513. Vaccine candidate *Brucella melitensis* 16M Δ*vjbR* is safe in a pregnant sheep model and confers protection. *mSphere*. **2020**;5(3).
 19. Russell-Lodrigue KE, Killeen SZ, Ficht TA, Roy CJ. Mucosal bacterial dissemination in a rhesus macaque model of experimental brucellosis. *J Med Primatol*. **2018**;47(1):75–77. Epub 20170602. doi: [10.1111/jmp.12282](https://doi.org/10.1111/jmp.12282). PubMed PMID: 28573738; PubMed Central PMCID: PMC65946315.
 20. Steinmeyer S, Howsmon DP, Alaniz RC, Hahn J, Jayaraman A. Empirical modeling of T cell activation predicts interplay of host cytokines and bacterial indole. *Biotechnol Bioeng*. **2017**;114(11):2660–2667. Epub 20170727. doi: [10.1002/bit.26371](https://doi.org/10.1002/bit.26371). PubMed PMID: 28667749; PubMed Central PMCID: PMC65614856.
 21. Krishnan S, Ding Y, Saeidi N, Choi M, Sridharan GV, Sherr DH, et al. Gut microbiota-derived tryptophan metabolites modulate inflammatory response in hepatocytes and macrophages *Cell Rep* **2019**;28:3285Epub 2019/09/19. doi: [10.1016/j.celrep.2019.08.080](https://doi.org/10.1016/j.celrep.2019.08.080). PubMed PMID: 31533048; PubMed Central PMCID: PMC6935324
 22. Singh NP, Singh UP, Rouse M, Zhang J, Chatterjee S, Nagarkatti PS, et al. Dietary indoles suppress delayed-type hypersensitivity by inducing a switch from pro-inflammatory Th17 cells to anti-inflammatory regulatory T cells through regulation of MicroRNA *J Immunol* **2016**;196:1108–1122Epub 2015/12/28. doi: [10.4049/jimmunol.1501727](https://doi.org/10.4049/jimmunol.1501727). PubMed PMID: 26712945
 23. Furusawa Y, Obata Y, Fukuda S, Endo TA, Nakato G, Takahashi D, et al. Commensal microbe-derived butyrate induces the differentiation of colonic regulatory T cells *Nature* **2013**;504:446–450Epub 2013/11/15. doi: [10.1038/nature12721](https://doi.org/10.1038/nature12721). PubMed PMID: 24226770
 24. Morgan ME, Flierman R, van Duivenvoorde LM, Witteveen HJ, van Ewijk W, van Laar JM, et al. Effective treatment of collagen-induced arthritis by adoptive transfer of CD25+ regulatory T cells. *Arthritis Rheum*. **2005**;52(7):2212–2221. doi:[10.1002/art.21195](https://doi.org/10.1002/art.21195).
 25. Sun G, Hou Y, Gong W, Liu S, Li J, Yuan Y, et al. Adoptive induced antigen-specific Treg cells reverse inflammation in collagen-induced arthritis mouse model. *Inflammation*. **2018**;41(2):485–495. doi:[10.1007/s10753-017-0704-4](https://doi.org/10.1007/s10753-017-0704-4).
 26. Haque M, Das JK, Xiong X, Song J. Targeting stem cell-derived tissue-associated regulatory T cells for type 1 diabetes immunotherapy. *Curr Diab Rep*. **2019**;19(10):89. Epub 2019/09/01. doi: [10.1007/s11892-019-1213-7](https://doi.org/10.1007/s11892-019-1213-7). PubMed PMID: 31471667; PubMed Central PMCID: PMC6830578.
 27. Haque R, Lei F, Xiong X, Bian Y, Zhao B, Wu Y, et al. Programming of regulatory T cells from pluripotent stem cells and prevention of autoimmunity *J Immunol* **2012**;189:1228–1236Epub 2012/06/27. doi: [10.4049/jimmunol.1200633](https://doi.org/10.4049/jimmunol.1200633). PubMed PMID: 22732595; PubMed Central PMCID: PMC63401327
 28. Yang JM, Ren Y, Kumar A, Xiong X, Das JK, Peng HY, et al. NAC1 modulates autoimmunity by suppressing regulatory T cell-mediated tolerance *Sci Adv* **2022**;8:eabo0183Epub 2022/06/30. doi: [10.1126/sciadv.abo0183](https://doi.org/10.1126/sciadv.abo0183). PubMed PMID: 35767626; PubMed Central PMCID: PMC69242588
 29. Fernandez-Prada CM, Zelazowska EB, Nikolich M, Hadfield TL, Roop RM 2nd, Robertson GL, et al. Interactions between *Brucella melitensis* and human phagocytes: bacterial surface O-Polysaccharide inhibits phagocytosis, bacterial killing, and subsequent host cell apoptosis. *Infect Immun*. **2003**;71(4):2110–2119. PubMed PMID: 12654833; PubMed Central PMCID: PMC6152029. doi:[10.1128/IAI.71.4.2110-2119.2003](https://doi.org/10.1128/IAI.71.4.2110-2119.2003).